International Journal of Engineering Science 226 (2026) 104579

Contents lists available at ScienceDirect

International Journal of Engineering Science

journal homepage: www.elsevier.com/locate/ijengsci

Full length article

Mechanical characterization of the murine reproductive tract during pregnancy and early postpartum recovery

Aileen C. Suarez [a], Kristin S. Miller [b], Kristin M. Myers [c], Steven D. Abramowitch [d], Raffaella De Vita [a,*]

[a] STRETCH Lab, Department of Mechanical Engineering, Virginia Tech, 325 Stanger Street, Blacksburg, 24061, VA, USA
[b] Department of Bioengineering, University of Texas Dallas, 2850 Rutford Ave, Richardson, 75080, TX, USA
[c] Department of Mechanical Engineering, Columbia University, 500 West 120th Street, New York City, 10027, NY, USA
[d] Department of Bioengineering, University of Pittsburgh, 3700 O'Hara Street, Pittsburgh, 15260, PA, USA

ARTICLE INFO

Keywords:
Pregnancy
Biomechanics
Remodeling

ABSTRACT

The female reproductive tract exhibits a remarkable capacity for extensive remodeling and large deformations during pregnancy. Despite its central role in reproduction, the mechanical adaptations of the entire tract remain poorly characterized. Here, we performed ex vivo inflation testing of the intact murine reproductive system, including the vagina, uterine body, and uterine horns, using non-contact, full-field deformation measurements to preserve anatomical continuity. This approach captured the collective mechanical response of the organ system across nonpregnant, late-pregnant, and three-week postpartum stages. Rupture pressure decreased from nonpregnant to late-pregnant tracts, with a partial increase by three weeks postpartum that remained below nonpregnant values. Late-pregnant tracts were markedly more distensible, with pressure–volume slopes an order of magnitude lower than those of nonpregnant and three-week postpartum tissues. Full-field strain mapping revealed region-specific behavior, with uterine regions deforming more than the vagina at moderate pressures during late pregnancy. At rupture pressures, the vagina was less extensible than uterine regions across nonpregnant, late-pregnant, and three-week postpartum conditions, with attenuated regional differences in late pregnancy. By three weeks postpartum, uterine regions had recovered strain levels comparable to the nonpregnant state, but the vagina continued to deform more at rupture pressure, indicating region-specific differences in recovery.

1. Introduction

Pregnancy is a remarkable example of regenerative medicine, representing a non-pathological state that orchestrates drastic yet precisely controlled changes throughout the human body. Over nine months, the female reproductive tract supports the transformation of a fertilized egg into a fully developed fetus. After birth, it rapidly begins reverting to its nonpregnant state, with the uterus returning to its pre-pregnancy size within six to eight weeks (Wachsberg et al., 1994), while other physiological changes (e.g., cervical involution McLaren, 1952, ovulation Jackson & Glasier, 2011, cardiovascular function Mahendru et al., 2014) may take longer (>twelve weeks) to recover. In response to elevated hormonal stimuli, the reproductive tract undergoes significant deformations, adapting biomechanical properties to support fetal development and facilitate birth (Baah-Dwomoh et al., 2016; Myers & Elad, 2017). However, the full extent of pregnancy-induced biomechanical remodeling is still poorly understood.

* Corresponding author.
E-mail address: devita@vt.edu (R. De Vita).

https://doi.org/10.1016/j.ijengsci.2026.104579
Received 1 April 2026; Received in revised form 16 May 2026; Accepted 17 May 2026

Collagen is the main structural protein in the uterus, cervix, and vagina, providing strength, stability, and support. Throughout pregnancy, collagen undergoes continuous remodeling, which is regulated by fibroblasts, smooth muscle cells, and immune cells that release growth factors, cytokines, and matrix-degrading enzymes (Colon-Caraballo et al., 2025; Jorge et al., 2014; Rossi et al., 2025). Mechanical forces and hormonal signals further modulate collagen degradation, fiber realignment, and cross-linking to meet the evolving demands of pregnancy in mice (Akins et al., 2011; Barnum et al., 2017; Nallasamy et al., 2017; Ouellette et al., 2022; Yoshida et al., 2014). In the human and rodent cervix, progressive collagen degradation and fiber disorganization facilitate softening and dilation (Aspden, 1988; Boyd et al., 2018; Byers et al., 2010), while in the uterus, collagen content increases in the mouse endometrium (Sanches et al., 2010; Teodoro et al., 2003) and collagen fibers straighten in the myometrium (Ouellette et al., 2022). Postpartum, dynamic collagen degradation is observed in humans (Woessner & Brewer, 1963) and rats (Harkness & Harkness, 1954); evidence suggests that the decrease in collagen during postpartum is associated with decreased tissue stiffness in the rodent cervix (Buhimschi et al., 2009; Harkness & Harkness, 1961; Yoshida et al., 2014).

It has been hypothesized that inadequate mechanical remodeling or recovery of reproductive tissues may contribute to adverse maternal outcomes such as preterm birth, birth injury, and possibly future pelvic floor disorders. Yet the mechanical basis of these potential links remains poorly defined. Human studies are limited by restricted access to reproductive tissues, especially at specific pregnancy and postpartum stages, and by the inability to control factors such as sample size, age, body composition, and parity. Even when tissues are available, they rarely capture the full range of mechanical states that occur across gestation, delivery, and recovery. These constraints make it challenging to obtain systematic measurements of distensibility and structural integrity, leaving significant gaps in our understanding of how reproductive tissues adapt mechanically during pregnancy and how insufficient adaptation might influence maternal health.

Animal models are commonly used to investigate the mechanical properties of reproductive tissues during pregnancy (Abramowitch et al., 2009; Baah-Dwomoh et al., 2016; Clark-Patterson et al., 2022; Dubik et al., 2025; Mitchell & Taggart, 2009; Yoshida et al., 2019). Mice and rats are especially prevalent because their short estrous cycles and brief gestation periods (19–21 days) allow progressive changes during pregnancy to be captured within a practical experimental window. They are also cost-effective, easy to handle, and exhibit reproductive tissues with organizational features that resemble those of humans (Aspden, 1988; Boyd et al., 2018). Despite their widespread use, the mechanical behavior of the murine reproductive system across pregnancy has not been systematically characterized. Rigorous quantification of how murine tissues mechanically adapt and remodel during gestation is needed, given the central role of mice as preclinical models for reproductive biology and for mechanistic studies that inform human pregnancy research.

Reproductive biomechanics studies have largely relied on ex vivo uniaxial mechanical testing, in which tissues are loaded along a single axis. This approach has been applied extensively to the vagina (Feola et al., 2011; Lowder et al., 2007; Rahn et al., 2008) and cervix (Barnum et al., 2017; Harkness & Harkness, 1959; Harkness & Nightingale, 1962; Jayyosi et al., 2018; Lee et al., 2022; Read et al., 2007; Yoshida et al., 2014, 2016). In late pregnancy, rat vaginas exhibit greater distension and higher ultimate strain while displaying reduced strength compared to virgin tissues (Feola et al., 2011; Lowder et al., 2007; Rahn et al., 2008). Their distensibility and strength return to virgin levels by three weeks postpartum (Feola et al., 2011; Lowder et al., 2007). The rat cervix also undergoes pronounced remodeling, showing increased distensibility (Harkness & Nightingale, 1962; Jayyosi et al., 2018; Lee et al., 2022) and reduced maximum load, stiffness, and stress relative to virgin cervices (Barnum et al., 2017; Harkness & Harkness, 1959; Read et al., 2007; Yoshida et al., 2014, 2016). Postpartum recovery occurs more rapidly in the cervix: stiffness returns to virgin values within 8 h of delivery (Barnum et al., 2017), and extensibility normalizes within 24 h (Harkness & Harkness, 1959, 1961). However, cervical strength decreases below virgin levels by 16 days postpartum (Harkness & Harkness, 1959, 1961). In contrast, fewer studies have examined the passive mechanical properties of the uterus across pregnancy, as research in this area has primarily focused on uterine contractility and intrauterine pressure during late gestation and delivery (Hollingsworth, 1975; Pierce et al., 2010; Robuck et al., 2018).

Uniaxial loading protocols, although widely used, do not reproduce the multidirectional deformation environment experienced by the reproductive tract in vivo. Biaxial inflation testing, in which internal pressurization induces circumferential and longitudinal deformation of the intact organ, provides a more physiologically relevant loading state by preserving native boundary conditions and the continuous extracellular matrix architecture that mediates load transfer, features disrupted when tissues are excised into strips. This approach also permits the vagina, cervix, and uterine horns to be examined as an integrated reproductive tract rather than as isolated regions. Inflation methods have been applied to the excised vagina (Akintunde et al., 2019; Dubik et al., 2022; McGuire et al., 2019, 2021; Robison et al., 2017; White et al., 2022) and to the uterocervical complex (Conway et al., 2019), but for pregnant rodents the available data are limited to a single ex vivo pressure–volume study (Downing et al., 2014) and one in vivo assessment of distensibility (Alperin et al., 2010). These studies did not resolve the spatially heterogeneous strain fields that develop across the reproductive tract during loading. In previous work (Dubik et al., 2024; McGuire et al., 2019, 2021), digital image correlation (DIC) enabled non-contact, full-field strain measurements during biaxial inflation, revealing localized mechanical responses such as tear propagation and creep in the virgin rat vagina. However, the mechanical behavior of the pregnant and postpartum vagina, cervix, and uterine horns—considered together as a continuous tract—under biaxial inflation remains unknown, constraining mechanistic understanding of how load is distributed through the reproductive system during gestation.

Here, we sought to determine how the mechanical properties of the entire murine reproductive tract change during pregnancy and postpartum by performing ex vivo inflation testing with non-contact, full-field deformation measurements. Building on prior MRI investigations of pregnancy-induced anatomical remodeling (Suarez et al., 2024), we examined mice at non-pregnant (NP), late-pregnant (LP), and three-weeks postpartum (3w PP) reproductive stages, which exhibit the most substantial geometric transformations and therefore represent informative points for assessing mechanical adaptation and recovery. Using a biaxial

Table 1
Median (IQR) values for animal characteristics and ex vivo reproductive tract dimensions of the tested specimens in NP (n = 9), LP (n = 9), and 3w PP (n = 9). Reported dimensions correspond to the geometry of the tissues at the time of mechanical testing following excision and specimen preparation, and therefore do not necessarily represent the in situ dimensions of the intact reproductive tract. Uterine horn thickness could be measured only at LP, since the organ was partially dissected prior to mechanical testing.

Median (IQR)	NP	LP	3w PP
Age (days)	98 (95–100)	104 (103–110)	132 (127–146)
Body weight (g)	36.52 (33.51–37.60)	65.84 (58.02–69.24)	37.01 (36.52–39.09)
Reproductive tract weight (g)	0.62 (0.55–0.69)	5.98 (5.62–6.27)	0.62 (0.48–0.66)
Uterine horn length (mm)	23.44 (22.52–25.79)	26.36 (23.21–27.70)	25.06 (24.56–30.52)
Uterine horn width (mm)	3.82 (2.70–3.87)	13.01 (12.45–14.05)	3.39 (3.11–3.66)
Uterine horn thickness (mm)	–	0.04 (0.04–0.04)	–
Uterine body length (mm)	6.86 (6.45–8.44)	13.02 (12.39–14.08)	6.89 (6.81–9.26)
Uterine body width (mm)	6.68 (6.16–7.31)	20.23 (19.33–21.12)	6.26 (5.73–7.05)
Cervix length (mm)	4.06 (3.96–4.44)	4.04 (3.75–4.68)	3.62 (3.45–3.64)
Cervix width (mm)	3.72 (3.66–4.11)	4.39 (3.98–4.79)	3.42 (3.38–3.45)
Vagina length (mm)	9.75 (9.40–9.90)	12.33 (11.61–14.58)	8.62 (8.22–9.19)
Vagina width (mm)	6.10 (5.64–6.21)	5.77 (4.96–6.05)	6.28 (5.67–6.68)
Vagina thickness (mm)	0.20 (0.18–0.28)	0.16 (0.12–0.21)	0.20 (0.18–0.20)
Number of pups	0	14 (12–16)	12 (12–13)

inflation setup, we quantified local strain distributions across the integrated tract until rupture under continuous saline infusion. We hypothesized that pregnancy would alter how mechanical deformation is distributed along the reproductive tract, leading to distinct regional strain patterns and markedly reduced rupture pressures compared to the non-pregnant state, and that postpartum tissues would exhibit only partial and region-dependent mechanical recovery. This study establishes foundational mechanical benchmarks for healthy murine pregnancy and postpartum remodeling, providing an integrated reference framework for future mechanistic and translational investigations of pregnancy-related disorders.

2. Experimental methods

2.1. Specimen preparation

All procedures were conducted in accordance with protocols approved by the Institutional Animal Care and Use Committee at Virginia Tech. Sexually mature female CD1 mice (Charles River; 3 months old at study onset) were allocated to nulliparous (NP; n = 9), late-pregnant (LP; gestation day 16–17; n = 9), and three-week postpartum (3w PP; n = 9) groups. Euthanasia was performed using CO_2 asphyxiation followed by cervical dislocation to ensure rapid and humane sacrifice (Fig. 1(a)). NP and 3w PP mice were euthanized during the estrous phase, verified by visual inspection of the vaginal opening (Byers et al., 2012). Carcasses were stored at 4 °C, and reproductive tracts were excised within 36 h of euthanasia. The entire tract, from the introitus to the ovarian fat pad, was isolated, and surrounding connective tissue and adipose layers were gently removed while preserving overall structural integrity. Samples were continuously hydrated with 1× phosphate-buffered saline (PBS) throughout dissection. Dimensional measurements were taken three times with a digital caliper and averaged for each animal, including the length and width of the uterine horn (oviduct to uterine body), uterine body, cervix, and vagina. Summary statistics (median (IQR)) for these dimensions, along with reproductive tract weights, body weights, litter size, and animal age, are provided in Table 1.

Reproductive tracts were stained with methylene blue for one hour before mounting. Each specimen was affixed to a syringe tip mounted on a 12-gauge stainless steel needle inserted through the introitus and secured over a rubber O-ring using nylon thread and Teflon tape (Fig. 1(b)). The mounted tracts were positioned on a 3D-printed pillar structure that maintained the tract in a single plane while allowing free extension during testing (Fig. 1(b)). For NP and 3w PP tracts, the distal ends of the uterine horns near the oviducts were closed with silk sutures. The same sutures were used to secure the reproductive tract to the supporting pillar. For LP specimens, the uterine horns were transected at the third implantation site and ligated with silk sutures, leaving two embryos in each horn to normalize uterine volume across pregnant tracts (Fig. 1(c), Table 1). All specimens were then speckled for DIC by applying a fine aerosol of fast-drying, gloss-white acrylic paint through a perforated metal sheet, producing a uniform non-contact strain measurement pattern.

2.2. Mechanical testing

Testing was performed using a custom-built inflation apparatus (Fig. 1(d)). Reproductive tracts were immersed in a room-temperature, PBS-filled acrylic tank with an optical window and connected via plastic tubing to a pressure transducer (maximum capacity: 15 psi ≈103 kPa; Omega Engineering Inc., Norwalk, CT) and a computer-controlled syringe pump (New Era Pump Systems Inc., Farmingdale, NY). Pressure signals were recorded and interfaced through a custom MATLAB (MathWorks, Natick, MA) script using an NI myDAQ data acquisition system (National Instruments, Austin, TX) (McGuire et al., 2019, 2021).

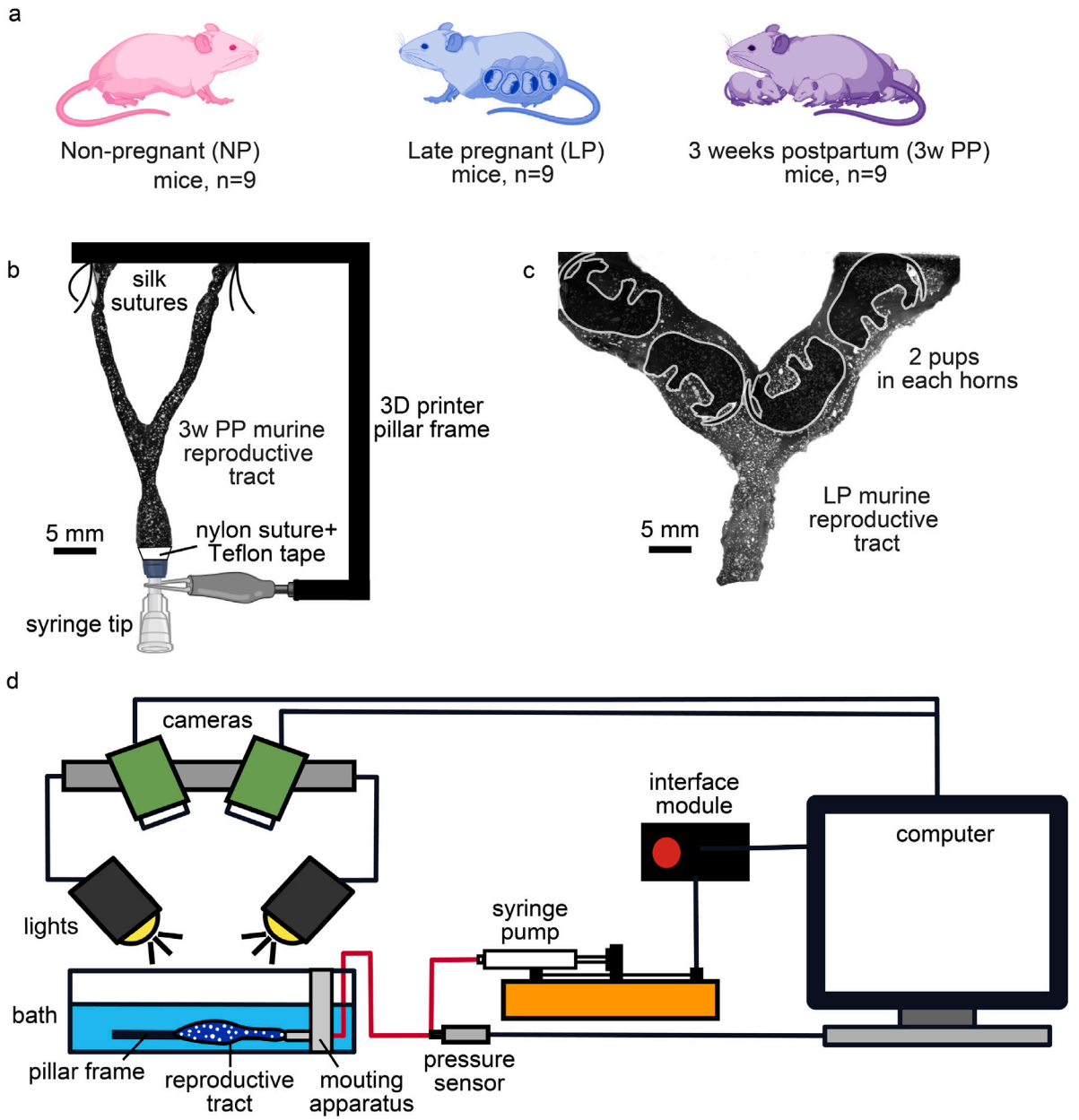

Fig. 1. (a) Representative timepoints used in this study: non-pregnant (NP), late-pregnant (LP), and three-week postpartum (3w PP). (b) Stained and speckled 3w PP reproductive tract shown in a DIC image, with schematic illustrations of the mounting elements: an O-ring at the introitus, syringe tip secured with nylon suture and Teflon tape, and a 3D-printed pillar supporting the uterine horns. (c) Stained and speckled LP reproductive tract shown in a DIC image, with embryos schematically represented within the uterine horns (two per side). (d) Schematic of the inflation testing apparatus showing its principal components.

Before testing, each specimen was preconditioned by ten inflation–deflation cycles of PBS to 6 kPa at a flow rate of 2 mL min^{-1}, using a custom closed-loop analog control interface and script (ANABOX 11, New Era Pump Systems Inc., Farmingdale, NY). After preconditioning, a preload of 2 kPa was applied before continuous pressurization with PBS at 2 mL min^{-1} until rupture.

Images were acquired at 4 Hz using two CMOS cameras (Basler ace A2440-75 um, Basler Inc., Exton, PA) fitted with C-mount lenses (Xenoplan 2.8/50, Schneider Optics Inc., Hauppauge, NY). Non-contact, full-field Lagrangian strain measurements were computed on the dorsal surface of the reproductive tract using a stereo 3D DIC system (Vic 3D 10, Correlated Solutions, Columbia, SC) (Fig. 1(d)). The DIC system was calibrated with a 12 × 9 grid pattern of 1 mm spacing and refined after testing using a hybrid calibration procedure. This hybrid method incorporated both rigid-grid and speckle-pattern images to correct for optical distortion

and refractive differences between air, the acrylic window, and PBS. These methods enabled quantification of infused volume, intraluminal pressure, and strain maps of the reproductive tract during inflation.

The slope of the linear portion of the pressure over volume infused curve was calculated from fitting a line to the data on Matlab with the function "polyfit". The maximum and minimum principal Lagrangian strains, e_1 and e_2, were computed using DIC by tracking the displacement and deformation of distinct subset regions within the speckle pattern on the reproductive tract surface. The principal strain angle, γ, was computed relative to the circumferential direction of the vagina, with 0° corresponding to alignment along this circumferential axis. This angle represents the orientation along which the maximum principal strain developed during inflation.

Strains were then averaged over small circular analysis regions positioned along the reproductive tract at the mid and proximal vagina, the caudal portion of the uterine body, the cranial portion of the uterine body near the inlet of one uterine horn, and along the uterine horn itself (Fig. 4). Two sites were evaluated within the uterine body because the caudal portion has a larger luminal cross-section than the cranial portion. In the pregnant reproductive tracts, the analysis region along the uterine horn was selected between adjacent embryos to minimize the influence of pre-existing local strains induced by the embryos.

To relate the orientation of the maximum principal strain to anatomical geometry, the longitudinal direction of the cranial uterine body and uterine horn was quantified using ImageJ (National Institutes of Health, Bethesda, MD). For each specimen, this direction was determined by measuring an angle between a line drawn along the circumferential direction of the vagina and a second line extending from the center of the uterine body through the midpoint of the uterine horn along its cylindrical axis. This anatomical angle defined the longitudinal axis of the uterine body and horn relative to the vaginal circumferential direction, serving as a reference for reporting the orientation of the maximum principal strain γ obtained from DIC analysis across reproductive stages.

2.3. Statistics

Statistical analyses were conducted in RStudio (version 2024.12.0) using generalized linear mixed models to compare selected pressure, slope, and strain metrics across the main fixed effects of region and reproductive stage, as well as their interaction. Statistical significance was defined as $p < 0.05$. Owing to the cross-sectional design, regional measurements within the same specimen and reproductive stage were treated as paired (repeated measures), whereas data from different reproductive stages were considered independent. Normality of residuals was assessed using the Shapiro–Wilk test and inspection of Q–Q plots with 95% confidence intervals, and homogeneity of variance was verified using Levene's test. Each variable was analyzed independently. Data skewness was evaluated with the "moments" package in RStudio. Raw data were used for the statistical analysis of rupture pressure and pressure–volume slopes. Strain data were transformed to reduce skewness using $\log(\text{value})$ for e_1 at 5 kPa and at rupture, $\log(\text{value} + 0.05)$ for e_2 at 5 kPa, and $\log(\text{value} + 0.13)$ for e_2 at rupture. When main or interaction effects were significant, post-hoc pairwise comparisons were performed using Tukey's honestly significant difference (HSD) test. For metrics with only one main effect (reproductive stage), such as rupture pressure and slope, Welch's ANOVA followed by Tukey's HSD was applied.

3. Results

Pressure–volume responses of murine reproductive tracts at NP, LP, and 3w PP under inflation to rupture are shown in Fig. 2(a), obtained using controlled infusion with a syringe pump and continuous pressure monitoring. The inflation response of the reproductive tract progressed through three stages: an initial compliant phase with substantial volume increase at low pressure, a stiffening phase characterized by rapid pressure escalation with continued volume loading, and rupture at peak inflation. Rupture pressures (median (IQR)) were 79.58 (14.32) kPa in NP tracts, 10.06 (4.04) kPa in LP tracts, and 37.15 (20.00) kPa in 3w PP tracts (Fig. 2(b)). The corresponding infused volumes (median (IQR)) were 2.71 (1.23) mL, 5.12 (3.24) mL, and 2.27 (0.89) mL, respectively. Rupture typically occurred at random sites along the uterine horns, away from the clamped vaginal introitus.

Because the reproductive stage significantly affected rupture pressure (Welch's ANOVA, $p = 9.92 \times 10^{-10}$), post-hoc pairwise comparisons were performed using Tukey's HSD test to evaluate differences between NP, LP, and 3w PP. Rupture pressure decreased significantly from NP to LP ($p = 4.43 \times 10^{-12}$), and increased considerably from LP to 3w PP ($p = 5.78 \times 10^{-6}$), with 3w PP reproductive tracts having rupture pressure values that were very different from the NP reproductive tracts ($p = 7.88 \times 10^{-7}$) (Fig. 2(b)).

The slope of the pressure–volume curve, a measure of the distensibility of the reproductive tract, was also compared across reproductive stages. A significant effect of the reproductive stage was observed (Welch's ANOVA, $p = 2.25 \times 10^{-8}$), which justified post hoc pairwise comparisons using Tukey's HSD. The median (IQR) slope for the reproductive tracts was 38.85 (5.33) Pa mL^{-1} for NP, 3.54 (0.74) Pa mL^{-1} for LP, and 32.92 (9.83) Pa mL^{-1} for 3w PP (Fig. 2(c)).

Images collected during testing were analyzed with stereo DIC to generate full-field deformation maps of the reproductive tract surface (Fig. 3). Maximum and minimum principal Lagrangian strains, denoted by e_1 and e_2, respectively, were reported, as they provide orientation-independent measures of tissue deformation. Principal strains were used because the tract's geometry transitions from a single vaginal canal to bifurcated uterine horns, precluding consistent definition of longitudinal and circumferential directions across the entire organ. As shown in Fig. 3, strain distribution was heterogeneous across the reproductive tract; uterine regions displayed greater strain than the vagina at comparable pressures, and this disparity became increasingly evident near rupture.

Strains were averaged within defined regions of interest located away from organ edges: mid vagina, proximal vagina, caudal uterine body, cranial uterine body, and uterine horn, as indicated in the schematic in Fig. 4. Fig. 4 illustrates the slightly nonlinear relationship between pressure and the maximum principal strain during inflation for five representative reproductive tracts, with measurements taken from the mid vagina, proximal vagina, caudal uterine body, cranial uterine body, and uterine

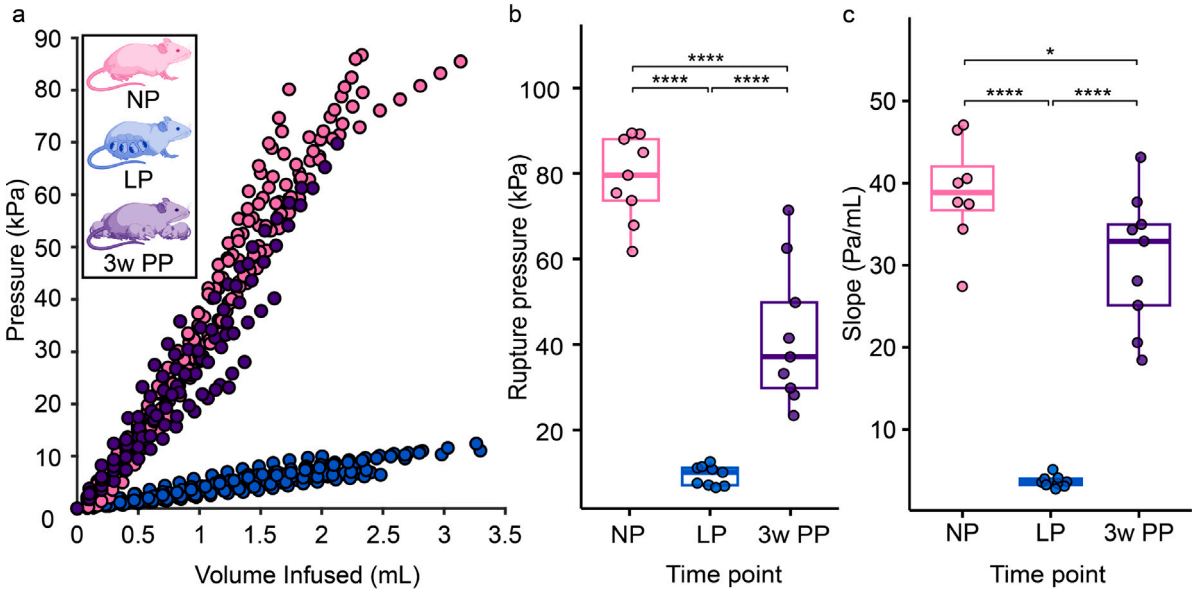

Fig. 2. (a) Pressure from pre-load up to rupture versus volume infused data for NP ($n = 9$), LP ($n = 9$), and 3w PP ($n = 9$) murine reproductive tracts. (b) Box plots of pressures at rupture (i.e., maximum pressures reported in (a)). (c) Box plots of the slopes of the pressure–volume curves reported in (a). $^{*}p < 0.05$, $^{****}p < 0.0001$.

horn. Qualitatively, one can observe that the NP (mid and proximal) vagina appeared to strain more at rupture compared to the LP and 3w PP vaginas (Fig. 4(a)–(b)). The uterine regions (caudal uterine body, cranial uterine body, and uterine horn) achieved larger strains than the vagina throughout our testing across all reproductive stages (Fig. 4(c)–(e)).

Fig. 5(a) shows e_1 at 5 kPa, a pressure attained by all specimens and used as a common basis for comparison across reproductive stages. Using a linear mixed model, no significant effects of region, reproductive stage, or their interaction on e_1 were detected ($p > 0.17$). At the 5 kPa pressure, the maximum principal strains in every region were higher in the LP tracts but not significantly higher than those experienced by the NP or 3w PP tracts.

The linear mixed model for e_2 at 5 kPa pressure shows that region has a significant effect ($p = 1.27 \times 10^{-4}$) as well as the interaction between reproductive stage and region ($p = 2.64 \times 10^{-14}$), suggesting that while reproductive stage alone did not affect e_2, pregnancy induced region-specific changes. The minimum principal strain, e_2, at the 5 kPa pressure for the proximal vagina in the LP tracts was significantly higher compared to the NP tracts. This strain measure for the caudal uterine body, cranial uterine body, and uterine horn regions was significantly higher in the LP tracts compared to the NP and 3w PP tracts (Fig. 5(b)). The caudal uterine body is the only region to exhibit lasting significant differences between NP and 3w PP. Interestingly, the minimum principal strains were often negative for the caudal uterine body in the NP tracts. Table 2 describes the significantly different relationships between regions from pairwise comparisons of e_1 and e_2 at 5 kPa pressure within each reproductive stage. The vaginal regions and the uterine regions appeared to reach very different minimum principal strains at 5 kPa pressure in the LP stage (Table 2).

Fig. 6(a) shows the maximum principal strain, e_1, at rupture pressure across reproductive tract regions. The linear mixed model revealed highly significant contributions of reproductive stage ($p = 1.57 \times 10^{-6}$), region ($p = 1.83 \times 10^{-15}$), and their interaction ($p = 6.15 \times 10^{-5}$) to variation in e_1 at rupture. The e_1 at rupture significantly decreased across all regions during pregnancy, from NP to LP. From LP to 3w PP, e_1 increased in all regions, returning to NP levels except in the proximal and mid vagina, where values at 3w PP remained significantly lower than NP. The uterine regions experienced the largest median e_1: 42% (IQR 18%) for uterine horn at NP, 8.6% (IQR 1.5%) for the caudal uterine body at LP, and 28% (IQR 16%) for the cranial uterine body at 3w PP (Fig. 6(a)). At each reproductive stage (NP, LP, and 3w PP), the vagina exhibited significantly lower maximum principal strain at rupture compared to the uterine regions (Table 2). This pattern was most pronounced in the NP and 3w PP groups, where both the mid and proximal vagina regions consistently showed lower strains than the caudal and cranial uterine body and uterine horn regions. At LP, the mid vagina exhibited a significantly lower e_1 than the uterine body.

The minimum principal strain, e_2, at rupture is reported for all regions of the reproductive tract in Fig. 6(b). The reproductive stage alone did not have a significant effect on e_2 at rupture ($p = 0.408$); however, significant differences in e_2 were observed across regions ($p = 2.25 \times 10^{-8}$) and in the interaction between reproductive stage and region ($p = 0.028$). At NP, rupture e_2 strains significantly varied among the (mid or proximal) vagina, cranial uterine body, and uterus. These regional differences were no longer evident at LP, and at 3w PP persisted only between the proximal vagina and uterine horn (Table 2).

The direction of the e_1, denoted by γ, at rupture in the (mid or proximal) vagina was aligned with the circumferential direction, with values ranging between −20° and 20° (Fig. 7), where 0° represents the circumferential direction. There were wider ranges of γ for the uterine regions. For the caudal uterine body, the γ angles at NP and 3w PP generally aligned to the circumferential

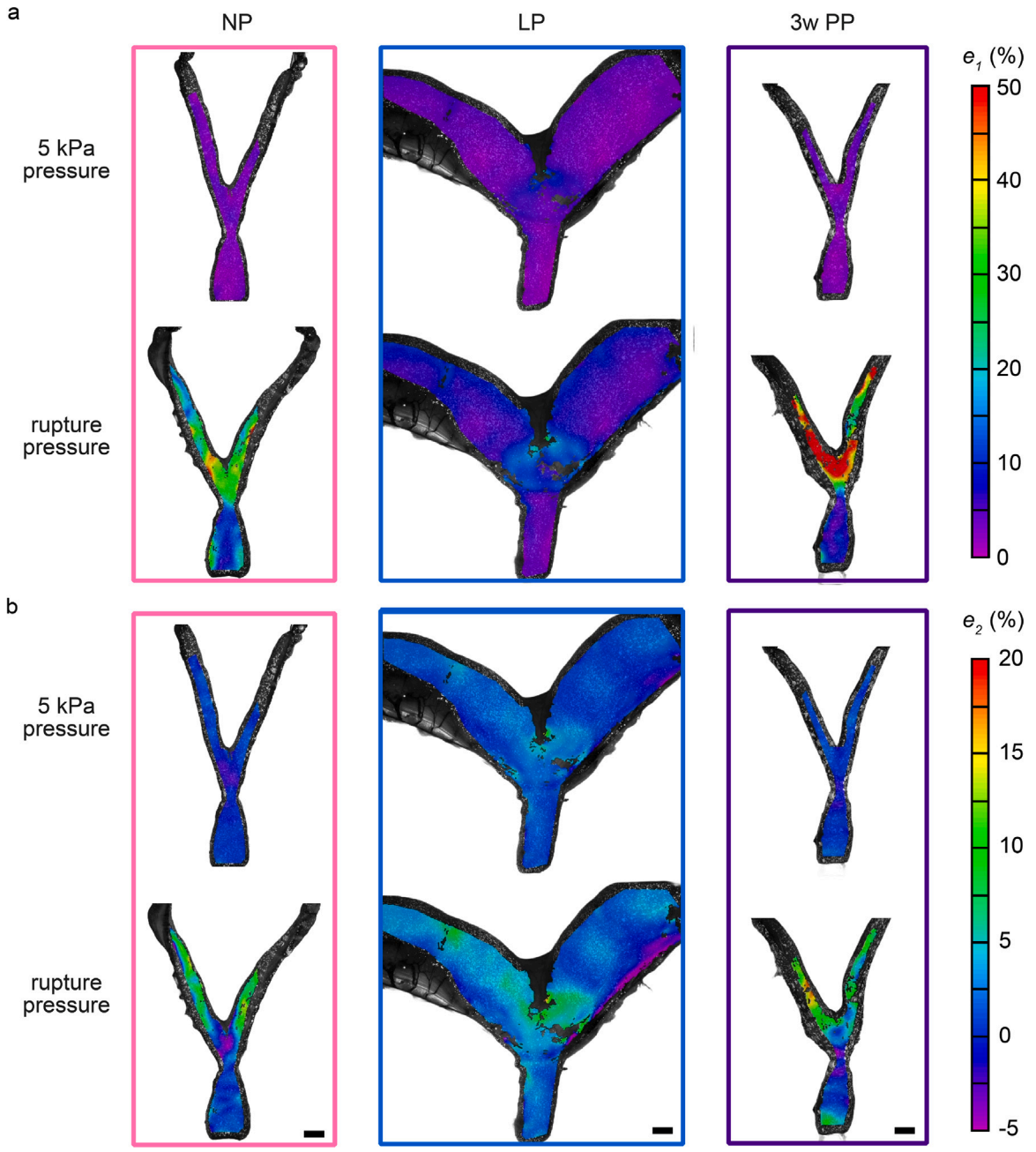

Fig. 3. (a) Maximum (e_1) and (b) minimum (e_2) principal Lagrangian strain maps of the surface of one NP, LP, and 3w PP murine reproductive tract at 5 kPa and rupture pressure. Scale bar is 5 mm.

direction of that region, but at LP more γ values were obliquely aligned between the circumferential and longitudinal directions. In the cranial uterine body and uterine horn regions, the γ angles appeared obliquely aligned between the circumferential and longitudinal directions at NP and 3w PP, while at LP γ aligned with the longitudinal direction. Note that the direction of e_2 was not reported, as it is by definition 90° from e_1.

4. Discussion

This study provides what is, to our knowledge, the first full-field characterization of deformation across the entire murine reproductive tract, including the vagina, cervix, and uterine horns, during controlled intraluminal pressurization. Our experimental

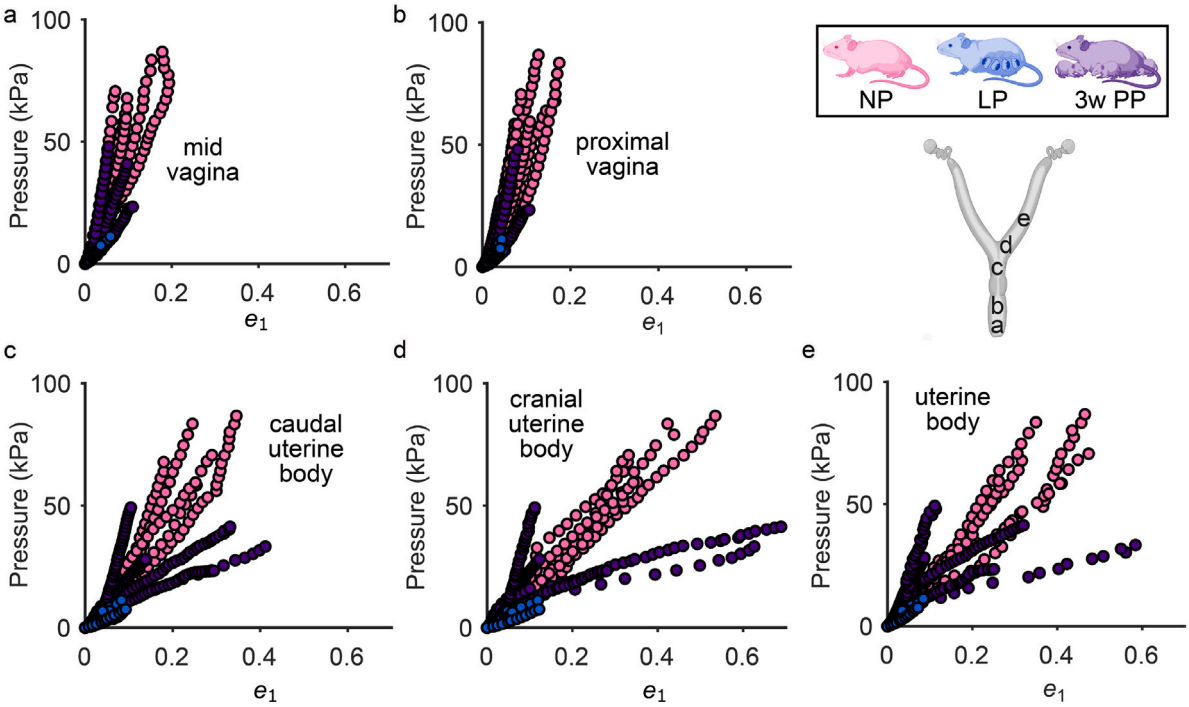

Fig. 4. Pressure versus maximum principal strains (e_1) computed in smaller regions of interest within the (a) mid vagina, (b) proximal vagina, (c) caudal uterine body, (d) cranial uterine body, and (e) uterine horn as shown in the schematic for five representative NP, LP, and 3w PP murine reproductive tracts.

Table 2
Statistically significant regional differences (mV: mid vagina, pV: proximal vagina, caUB: caudal uterine body, crUB: cranial uterine body, and UH: uterine horn) in maximum (e_1) and minimum (e_2) principal strains at 5 kPa and at rupture pressure across three reproductive stages (NP, LP, 3w PP).

Principal strains	NP	LP	3w PP
e_1 at 5 kPa pressure	–	–	–
e_2 at 5 kPa pressure	mV:caUB** caUB:UH**	mV:caUB**** mV:crUB**** mV:UH*** pV:caUB**** pV:crUB**** pV:UH*	–
e_1 at rupture pressure	mV:caUB*** mV:crUB**** mV:UH**** pV:caUB* pV:crUB*** pV:UH****	mV:caUB** mV:crUB**	mV:caUB**** mV:crUB**** mV:UH**** pV:caUB**** pV:crUB**** pV:UH****
e_2 at rupture pressure	mV:crUB* mV:UH** pV:crUB*** pV:UH**** caUB:UH*	–	pV:UH*

Significance by Tukey's HSD:
* $p < 0.05$.
** $p < 0.01$.
*** $p < 0.001$.
**** $p < 0.0001$.

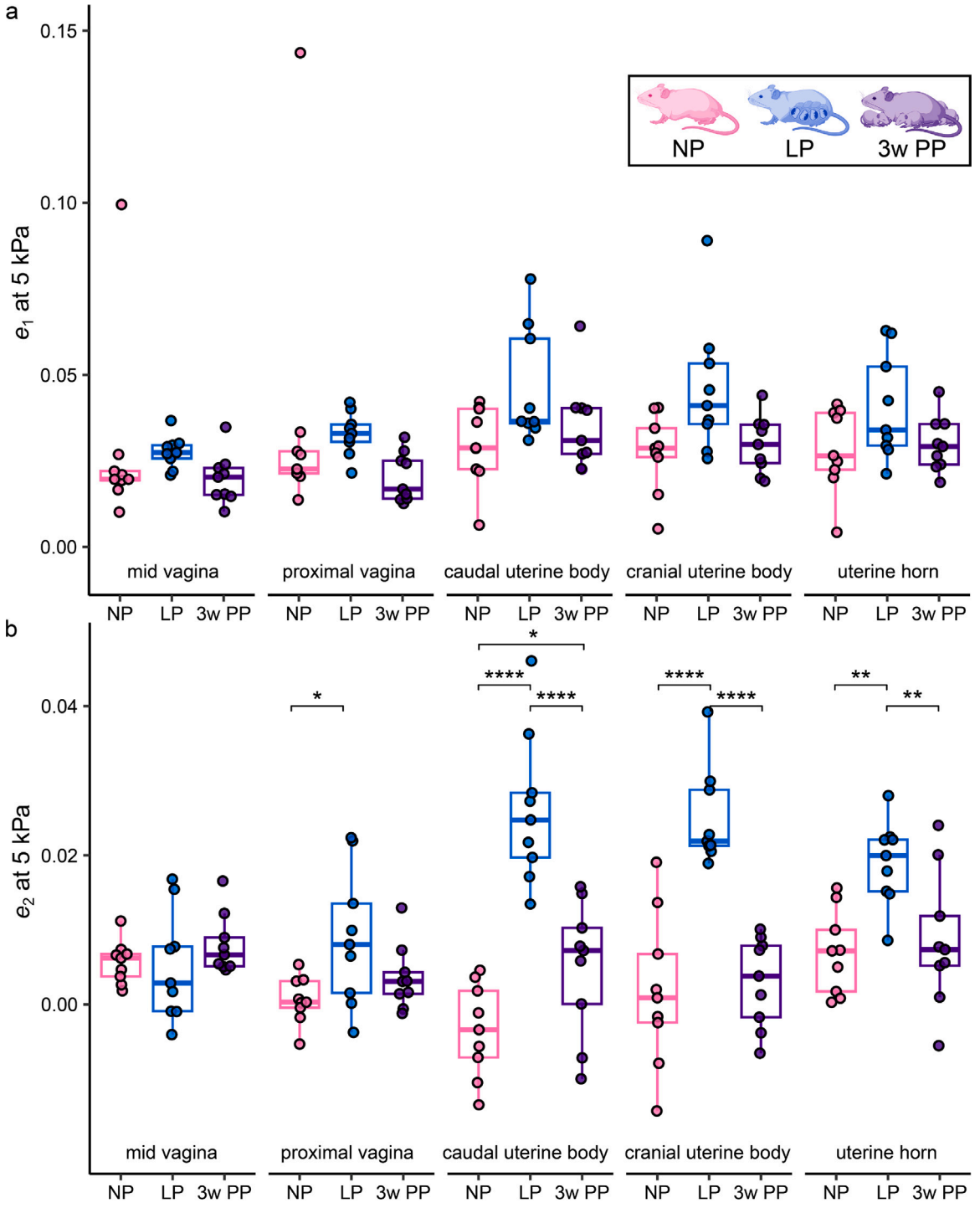

Fig. 5. Box plots of the (a) maximum principal strains (e_1) and (b) minimum principal strains (e_2) at 5 kPa pressure computed in different regions of NP ($n = 9$), LP ($n = 9$), and 3w PP ($n = 9$) murine reproductive tracts. $^{*}p < 0.05$, $^{**}p < 0.01$, $^{***}p < 0.001$, $^{****}p < 0.0001$.

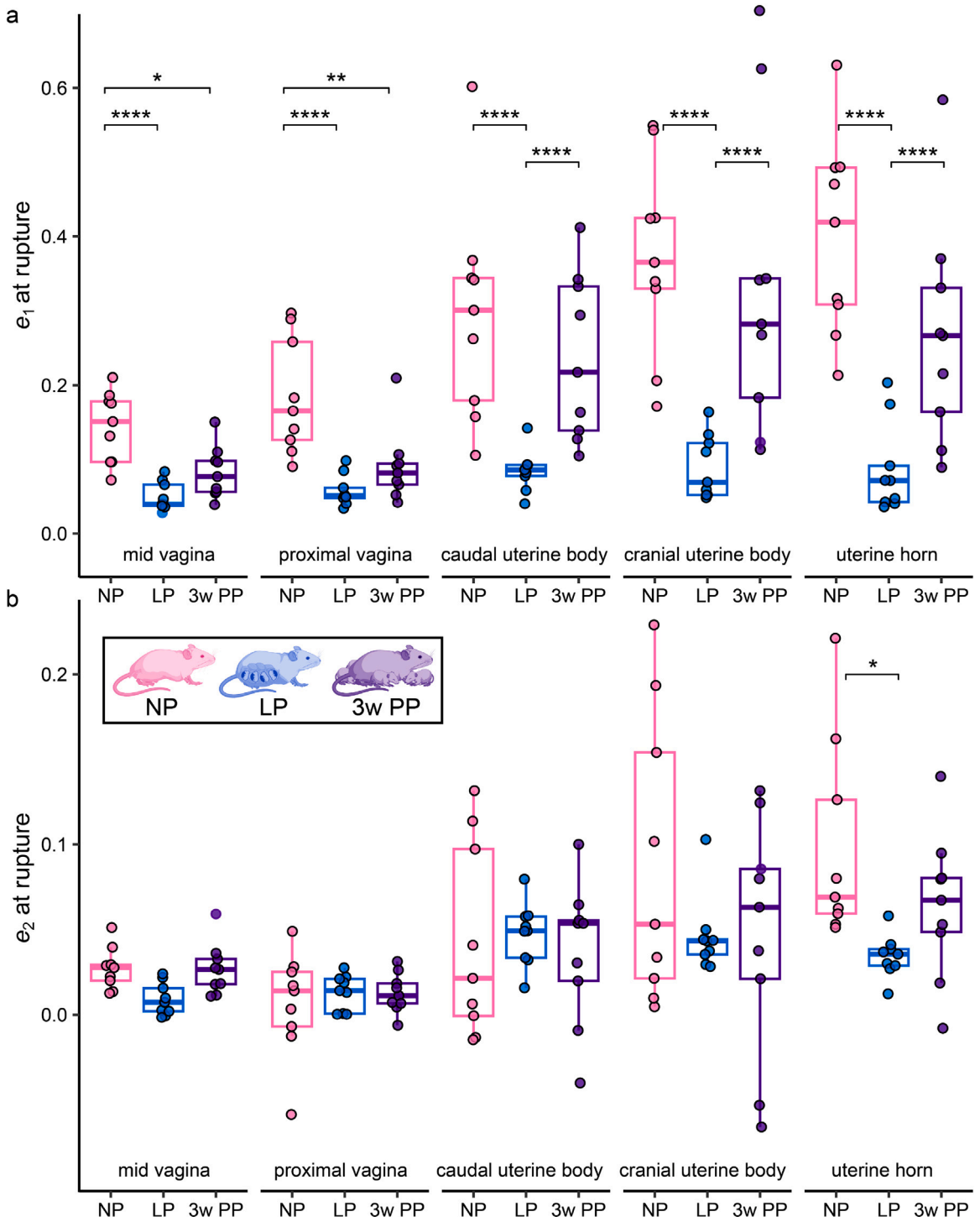

Fig. 6. Box plots of the (a) maximum principal strains (e_1) and (b) minimum principal strains (e_2) at rupture computed in different regions of NP ($n = 9$), LP ($n = 9$), and 3w PP ($n = 9$) murine reproductive tracts. $^{*}p < 0.05$, $^{**}p < 0.01$, $^{***}p < 0.001$, $^{****}p < 0.0001$.

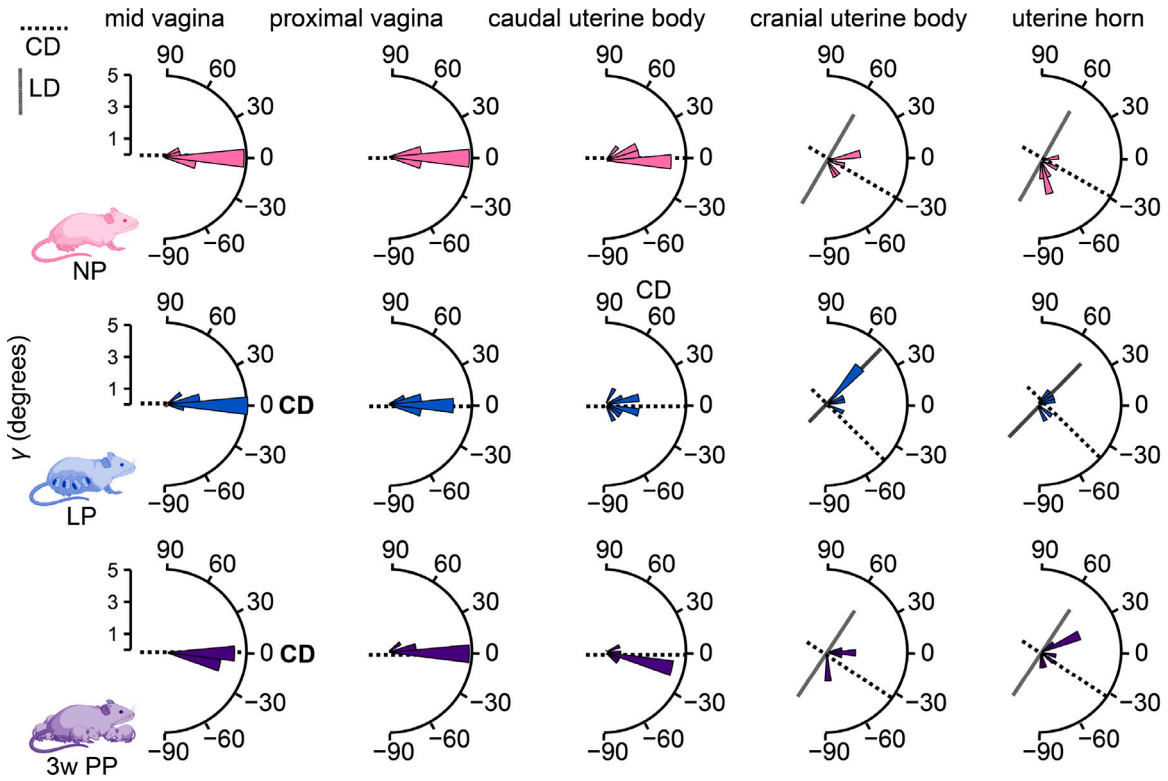

Fig. 7. Polar histograms of the direction of maximum principal strain, γ, in degrees at rupture for each region (mid vagina, proximal vagina, caudal uterine body, cranial uterine body, and uterine horn) and reproductive stage (NP, LP, and 3w PP). The frequency of the angular bins represents the number of reproductive tracts. The thick dashed lines represent the approximate circumferential direction (CD), and the thin, dense dashed lines represent the longitudinal direction (LD) of each region.

design enabled the tract to be pressurized as an integrated structure while preserving its overall geometry, allowing deformation to unfold according to the tract's natural anatomical continuity. Full-field strain measurements obtained using DIC captured how the tract responded mechanically throughout inflation. We anticipated that pregnancy would significantly alter deformation patterns along the reproductive tract by reducing global rupture resistance, increasing global distensibility, and producing distinct regional strain responses, and that postpartum tissues would regain mechanical function only partially and in a region-specific manner. The results are consistent with these expectations, revealing substantial softening during late pregnancy and a heterogeneous pattern of mechanical recovery by three weeks postpartum.

The pressure required to rupture specimens at each reproductive stage (Fig. 2(a)–(b)) and the slopes of the linear region of the pressure–volume curves (Fig. 2(c)) indicate that pregnancy and early postpartum produce lasting alterations in reproductive tract mechanics. LP specimens exhibited significantly lower rupture pressures and smaller slopes, reflecting reduced strength and stiffness at this gestational stage, consistent with prior studies of the murine vagina (Feola et al., 2011; Lowder et al., 2007; Rahn et al., 2008) and cervix (Barnum et al., 2017; Harkness & Harkness, 1959; Read et al., 2007; Yoshida et al., 2014, 2016). The significant differences observed between NP and 3w PP specimens diverge somewhat from rat studies reporting a return to NP mechanical behavior by 2–4 weeks postpartum; however, these findings may indicate species-specific differences in the timing or extent of postpartum remodeling, as murine recovery trajectories may not parallel those reported in rats.

The full-field strain maps revealed regional deformation patterns that pressure–volume measurements could not resolve (Fig. 3). Maximum and minimum principal strains were used to compare deformation across reproductive regions because the tract's curved and anatomically distinct structures do not share a common coordinate system. As expected, maximum principal strain increased with pressure in both the vaginal and uterine regions (Fig. 4). The variation observed in the pressure–strain response across animals reflects differences in overall uterine and vaginal size, wall thickness, and pregnancy-related remodeling (Table 1), rather than differences in organ shape within a single tract.

At a pressure of 5 kPa, well below uterine rupture, the maximum principal strain (e_1) did not differ statistically across regions (mid vagina, proximal vagina, caudal uterine body, cranial uterine body, and uterine horn)) and stages (NP, LP, and 3w PP) (Fig. 5(a), Table 2, first row). Early large deformation of the reproductive tract emerges as a coordinated, tract-wide response rather than as a set of region-specific behaviors, consistent with the integrated load sharing and structural continuity of the organ system. However, the minimum principal strain (e_2) in the (cranial and caudal) uterine body and uterine horns was remarkably higher than in the (mid and proximal) vagina (Fig. 5(b), Table 2, second row) in late pregnancy. Overall, the LP tracts exhibited higher e_1 and

e_2 than the NP and 3w PP tract (Fig. 5(a)–(b)), indicating increased compliance across different regions. The uterine regions not only deformed more than the vagina, as demonstrated by a higher e_2, but exhibited more pronounced and statistically significant differences between NP and LP and between LP and 3w PP, whereas NP and 3w PP uterine specimens showed a more similar response (Fig. 5(b)). These data indicate that pregnancy induces a transient reorganization of uterine mechanical function, softening and deforming more readily to accommodate fetal growth. Within several weeks postpartum, the uterus transitions back toward its nonpregnant mechanical state as the compliance of the uterine body and horns largely recovered to NP levels (Fig. 5).

The specimens failed at various pressures across reproductive stages and rupture largely occurred at the uterine horns, suggesting that the uterine horns may have a lower strength compared to the vagina (Figs. 2(a)–(b) and 4). When comparing the maximum principal strain (e_1) values at rupture for each region (mid and proximal vagina, caudal and cranial uterine body, and uterine horns) across reproductive stages, all regions significantly differed between NP and LP (Fig. 6(a)). At 3w PP, the e_1 values at rupture recovered for all uterine regions such that the average strains were higher than their LP counterparts, but were not statistically different from the NP counterparts. In contrast, the vaginal regions did have a significant difference between NP and 3w PP when comparing e_1 values at rupture.

Due to their tubular geometry, the vaginal regions consistently exhibited maximum principal strain (e_1) along the circumferential direction at all reproductive stages (Fig. 7), consistent with prior work (Akintunde et al., 2019; Dubik et al., 2022; McGuire et al., 2019; Robison et al., 2017; White et al., 2022). The caudal uterine body showed a similar pattern at the NP stage, but in late pregnancy the strain field rotated, and e_1 no longer aligned with the circumferential direction (Fig. 7). In the cranial uterine body and uterine horns at LP, measurements of maximum principal strain (and associated directions) were obtained between implantation sites, where the tissue was not prestretched by embryo loading. In these regions, pregnancy-induced remodeling appears to have reduced the effective stiffness along the longitudinal direction more than along the circumferential direction. Consequently, when pressurized, the tissue deformed preferentially along the mechanically softer longitudinal direction, which is the direction of e_1 in these regions. This behavior is consistent with the remarkable longitudinal growth of the uterine horns during late pregnancy (Suarez et al., 2024), as each horn expands to accommodate multiple developing fetuses arranged sequentially along its length. Such expansion likely alters tissue architecture and mechanical anisotropy, thereby increasing compliance along the longitudinal direction and promoting preferential deformation along this axis under pressurization. Further studies are needed to determine how pregnancy-associated remodeling modifies the underlying tissue microstructure and contributes to these changes in mechanical behavior.

A pressure of 5 kPa was used because all reproductive tracts reached this level, even though it exceeds reported intrauterine pressures during parturition in mice (~2.5–4 kPa Pierce et al., 2010). Strain magnitudes measured here are larger than those reported in other studies of murine reproductive tissues, largely due to differences in testing modality (e.g., inflation to failure with full-field DIC strain mapping in the present study, rather than the inflation–extension protocol and discrete marker-based strain measurements used previously) (Akintunde et al., 2019; Robison et al., 2017; White et al., 2022). The only other study to compare mechanical behavior across organs within the reproductive tract (limited to the NP state) is by Conway et al. (2019), who found the cervix to be stiffer than the uterine horn. We did not quantify cervical strain because the cervix resides within the interior of the tract and is not visible on the external surface used for strain mapping. However, if the proximal vagina and caudal uterine body reproduce even part of the cervix's mechanical response (Table 2, first row), our observations align with the difference in elastic moduli reported by Conway and colleagues (Conway et al., 2019).

Several aspects of the experimental configuration influence how the results should be interpreted. The volume–pressure curves require cautious interpretation, as the infused volume may differ from the retained luminal volume due to the permeability of reproductive tissues. Pressure was measured at the introitus and assumed to be uniform along the tract; estimates of lumen radii suggest that any pressure drop between the vagina and uterine horns would be on the order of only 5 Pa, negligible relative to the applied loads. Because DIC captures deformation only on the external speckled surface, internal wall deformation and through-thickness strain could not be resolved. Although both pressure and strain were measured, regional stresses could not be calculated because wall-thickness changes during inflation (or prior to inflation) in every region was not measured to keep the reproductive tract intact. This limitation affects stress-based comparisons but does not impact the surface strain fields obtained through DIC. Finally, the LP uterine horns could not be inflated after embryo removal because the tissue collapsed on itself, preventing accurate strain tracking for the entire duration of the test starting in this configuration; the presence of embryos therefore influenced the LP uterine measurements, even though strains were assessed between implantation sites.

5. Conclusion

This work presents an experimental framework for quantifying finite deformations across the mouse reproductive tract and establishes baseline mechanical characteristics of pregnancy and postpartum remodeling. Distensibility and strength declined considerably at late pregnancy and did not fully recover by three weeks postpartum, with the uterine horns exhibiting the greatest deformation capacity across stages. These measurements show how pregnancy alters the mechanical behavior of the tract and provide a platform for probing region-specific remodeling in future studies. The methods and findings offer a foundation for evaluating murine pregnancy as a preclinical model and for generating mechanistic hypotheses relevant to human reproductive health.

CRediT authorship contribution statement

Aileen C. Suarez: Writing – review & editing, Writing – original draft, Visualization, Validation, Methodology, Investigation, Formal analysis, Data curation, Conceptualization. **Kristin S. Miller:** Writing – review & editing, Funding acquisition, Conceptualization. **Kristin M. Myers:** Writing – review & editing, Funding acquisition, Conceptualization. **Steven D. Abramowitch:** Writing – review & editing, Funding acquisition, Conceptualization. **Raffaella De Vita:** Writing – review & editing, Writing – original draft, Visualization, Supervision, Resources, Project administration, Methodology, Investigation, Funding acquisition, Formal analysis, Data curation, Conceptualization.

Declaration of competing interest

The authors declare the following financial interests/personal relationships which may be considered as potential competing interests: Raffaella De Vita reports a relationship with Editorial board of the IJES that includes: board membership. Given her role as a member of the editorial board of this journal, R. De Vita had no involvement in the peer review of this article and had no access to information regarding its peer review. Full responsibility for the editorial process for this article was delegated to another journal editor. The other authors declare that they have no known competing financial interests or personal relationships that could have appeared to influence the work reported in this paper.

Acknowledgement

Funding was provided by the National Science Foundation under Grant No. 2053851.

Data availability

The datasets collected and analyzed during the current study are available from the corresponding author on reasonable request.

References

Abramowitch, S. D., Feola, A., Jallah, Z., & Moalli, P. A. (2009). Tissue mechanics, animal models, and pelvic organ prolapse: a review. *European Journal of Obstetrics, Gynecology, and Reproductive Biology*, *144*, S146–S158. http://dx.doi.org/10.1016/j.ejogrb.2009.02.022.

Akins, M. L., Luby-Phelps, K., Bank, R. A., & Mahendroo, M. (2011). Cervical softening during pregnancy: Regulated changes in collagen cross-linking and composition of matricellular proteins in the mouse. *Biology of Reproduction*, *84*, 1053–1062. http://dx.doi.org/10.1095/biolreprod.110.089599.

Akintunde, A. R., Robison, K. M., Capone, D. J., Desrosiers, L., Knoepp, L. R., & Miller, K. S. (2019). Effects of elastase digestion on the murine vaginal wall biaxial mechanical response. *Journal of Biomechanical Engineering*, *141*, Article 0210111. http://dx.doi.org/10.1115/1.4042014.

Alperin, M., Feola, A., Duerr, R., Moalli, P., & Abramowitch, S. (2010). Pregnancy- and delivery-induced biomechanical changes in rat vagina persist postpartum. *International Urogynecology Journal*, *21*, 1169–1174. http://dx.doi.org/10.1007/s00192-010-1149-6.

Aspden, R. M. (1988). Collagen organisation in the cervix and its relation to mechanical function. *Collagen and Related Research*, *8*, 103–112. http://dx.doi.org/10.1016/s0174-173x(88)80022-0.

Baah-Dwomoh, A., McGuire, J., Tan, T., & De Vita, R. (2016). Mechanical properties of female reproductive organs and supporting connective tissues: a review of the current state of knowledge. *Applied Mechanics Reviews*, *68*, http://dx.doi.org/10.1115/1.4034442.

Barnum, C. E., Fey, J. L., Weiss, S. N., Barila, G., Brown, A. G., Connizzo, B. K., Shetye, S. S., Elovitz, M. A., & Soslowsky, L. J. (2017). Tensile mechanical properties and dynamic collagen fiber re-alignment of the murine cervix are dramatically altered throughout pregnancy. *Journal of Biomechanical Engineering*, *139*, Article 0610081. http://dx.doi.org/10.1115/1.4036473.

Boyd, K. L., Muehlenbachs, A., Rendi, M. H., Garcia, R. L., & Gibson-Corley, K. N. (2018). *Comparative anatomy and histology: Chapter 17 female reproductive sysytem*. Elsevier Inc., http://dx.doi.org/10.1016/B978-0-12-802900-8.00017-8.

Buhimschi, C. S., Sora, N., Zhao, G., & Buhimschi, I. A. (2009). Genetic background affects the biomechanical behavior of the postpartum mouse cervix. *American Journal of Obstetrics and Gynecology*, *200*, 434.e1–434.e7. http://dx.doi.org/10.1016/j.ajog.2008.11.005.

Byers, B. D., Bytautiene, E., Costantine, M. M., Buhimschi, C. S., Buhimschi, I., Saade, G. R., & Goharkhay, N. (2010). Hyaluronidase modifies the biomechanical properties of the rat cervix and shortens the duration of labor independent of myometrial contractility. *American Journal of Obstetrics and Gynecology*, *203*, 596.e1–596.e5. http://dx.doi.org/10.1016/j.ajog.2010.07.031.

Byers, S. L., Wiles, M. V., Dunn, S. L., & Taft, R. A. (2012). Mouse estrous cycle identification tool and images. *PLOS One*, *7*(4), e35538. http://dx.doi.org/10.1371/journal.pone.0035538.

Clark-Patterson, G., Domingo, M., & Miller, K. S. (2022). Biomechanics of pregnancy and vaginal delivery. *Current Opinion in Biomedical Engineering*, *22*, Article 100386. http://dx.doi.org/10.1016/j.cobme.2022.100386.

Colon-Caraballo, M., Russell, S. R., Myers, K. M., & Mahendroo, M. (2025). Collagen turnover during cervical remodeling involves both intracellular and extracellular collagen degradation pathways. *Biology of Reproduction*, *112*, 709–727. http://dx.doi.org/10.1093/biolre/ioaf012.

Conway, C. K., Qureshi, H. J., Morris, V. L., Danso, E. K., Desrosiers, L., Knoepp, L. R., Goergen, C. J., & Miller, K. S. (2019). Biaxial biomechanical properties of the nonpregnant murine cervix and uterus. *Journal of Biomechanics*, *94*, 39–48. http://dx.doi.org/10.1016/j.jbiomech.2019.07.011, arXiv:31353018.

Downing, K. T., Billah, M., Raparia, E., Shah, A., Silverstein, M. C., Ahmad, A., & Boutis, G. S. (2014). The role of mode of delivery on elastic fiber architecture and vaginal vault elasticity: A rodent model study. *Journal of the Mechanical Behavior of Biomedical Materials*, *29*, 190–198. http://dx.doi.org/10.1016/j.jmbbm.2013.08.025.

Dubik, J., Alperin, M., & De Vita, R. (2025). The biomechanics of the vagina: a complete review of incomplete data. *NPJ Women's Health*, *3*, 4. http://dx.doi.org/10.1038/s44294-024-00047-7.

Dubik, J., Tartaglione, A., Miller, K. S., Dillard, D. A., & De Vita, R. (2022). History-dependent deformations of rat vaginas under inflation. *Integrative and Comparative Biology*, *62*, 625–640. http://dx.doi.org/10.1093/icb/icac110.

Dubik, J., Tartaglione, A., Wineman, A., Dillard, D., & De Vita, R. (2024). A finite strain integral model for the creep behavior of vaginal tissue. *International Journal of Non-Linear Mechanics*, *162*, Article 104729. http://dx.doi.org/10.1016/j.ijnonlinmec.2024.104729.

Feola, A., Moalli, P., Alperin, M., Duerr, R., Gandley, R. E., & Bramowitch, S. (2011). Impact of pregnancy and vaginal delivery on the passive and active mechanics of the rat vagina. *Annals of Biomedical Engineering*, *39*, 549. http://dx.doi.org/10.1007/s10439-010-0153-9.

Harkness, M. L. R., & Harkness, R. D. (1954). The collagen content of the reproductive tract of the rat during pregnancy and lactation. *Journal of Physiology*, *123*, 492. http://dx.doi.org/10.1113/jphysiol.1954.sp005066.

Harkness, M. L., & Harkness, R. D. (1959). Changes in the physical properties of the uterine cervix of the rat during pregnancy. *Journal of Physiology*, *148*, 524–547. http://dx.doi.org/10.1113/jphysiol.1959.sp006304.

Harkness, M. L. R., & Harkness, R. D. (1961). The mechanical properties of the uterine cervix of the rat during involution after parturition. *Journal of Physiology*, *156*, 112. http://dx.doi.org/10.1113/jphysiol.1961.sp006661.

Harkness, R. D., & Nightingale, M. A. (1962). The extensibility of the cervix uteri of the rat at different times of pregnancy. *Journal of Physiology*, *160*, 214. http://dx.doi.org/10.1113/jphysiol.1962.sp006842.

Hollingsworth, M. (1975). Mechanical responses of rat isolated uterine horns to transmural stimulation. *British Journal of Pharmacology*, *55*, 41. http://dx.doi.org/10.1111/j.1476-5381.1975.tb07607.x.

Jackson, E., & Glasier, A. (2011). Return of ovulation and menses in postpartum (nonlactating) women: A systematic review. *Obstetrics & Gynecology*, *117*, 657–662. http://dx.doi.org/10.1097/AOG.0b013e31820ce18c.

Jayyosi, C., Lee, N., Willcockson, A., Nallasamy, S., Mahendroo, M., & Myers, K. (2018). The mechanical response of the mouse cervix to tensile cyclic loading in term and preterm pregnancy. *Acta Biomaterials*, *78*, 308–319. http://dx.doi.org/10.1016/j.actbio.2018.07.017.

Jorge, S., Chang, S., Barzilai, J., Leppert, P., & Segars, J. (2014). Mechanical signaling in reproductive tissues. *Reproduction Science*, *21*, http://dx.doi.org/10.1177/1933719114542023.

Lee, N., Shi, L., Caraballo, M. C., Nallasamy, S., Mahendroo, M., Iozzo, R. V., & Myers, K. (2022). Mechanical response of mouse cervices lacking decorin and biglycan during pregnancy. *Journal of Biomechanical Engineering*, *144*, http://dx.doi.org/10.1115/1.4054199.

Lowder, J. L., Debes, K. M., Moon, D. K., Howden, N., Abramowitch, S. D., & Moalli, P. A. (2007). Biomechanical adaptations of the rat vagina and supportive tissues in pregnancy to accommodate delivery. *Obstetrics and Gynecology*, *109*, 136–143. http://dx.doi.org/10.1097/01.aog.0000250472.96672.6c.

Mahendru, A. A., Everett, T. R., Wilkinson, I. B., Lees, C. C., & McEniery, C. M. (2014). A longitudinal study of maternal cardiovascular function from preconception to the postpartum period. *Journal of Hypertension*, *32*, 849–856. http://dx.doi.org/10.1097/HJH.0000000000000090.

McGuire, J. A., Crandall, C. L., Abramowitch, S. D., & De Vita, R. (2019). Inflation and rupture of vaginal tissue. *Interface Focus*, *9*, Article 20190029. http://dx.doi.org/10.1098/rsfs.2019.0029.

McGuire, J. A., Monclova, J. L., Coariti, A. C. S., Stine, C. A., Toussaint, K. C., Jr., Munson, J. M., Dillard, D. A., & De Vita, R. (2021). Tear propagation in vaginal tissue under inflation. *Acta Biomaterials*, *127:193-204*, 193–204. http://dx.doi.org/10.1016/j.actbio.2021.03.065.

McLaren, H. C. (1952). The involution of the cervix. *BMJ*, *1*, 347–352. http://dx.doi.org/10.1136/bmj.1.4754.347.

Mitchell, B. F., & Taggart, M. J. (2009). Are animal models relevant to key aspects of human parturition? *American Journal of Physiology-Regulatory, Integrative and Comparative Physiology*, http://dx.doi.org/10.1152/ajpregu.00153.2009.

Myers, K. M., & Elad, D. (2017). Biomechanics of the human uterus. *WIREs Systems Biology and Medicine*, *9*, Article e1388. http://dx.doi.org/10.1002/wsbm.1388.

Nallasamy, S., Yoshida, K., Akins, M., Myers, K., Iozzo, R., & Mahendroo, M. (2017). Steroid hormones are key modulators of tissue mechanical function via regulation of collagen and elastic fibers. *Endocrinology*, *158*, 950–962. http://dx.doi.org/10.1210/en.2016-1930.

Ouellette, A., Mahendroo, M., & Nallasamy, S. (2022). Collagen and elastic fiber remodeling in the pregnant mouse myometrium. *Biology of Reproduction*, *107*, 741–751. http://dx.doi.org/10.1093/biolre/ioac102.

Pierce, S. L., Kutschke, W., Cabeza, R., & England, S. K. (2010). In vivo measurement of intrauterine pressure by telemetry: a new approach for studying parturition in mouse models. *Physiological Genomics*, *42*, 310–316. http://dx.doi.org/10.1152/physiolgenomics.00058.2010.

Rahn, D. D., Ruff, M. D., Brown, S. A., Tibbals, H. F., & Word, R. A. (2008). Biomechanical properties of the vaginal wall: effect of pregnancy, elastic fiber deficiency, and pelvic organ prolapse. *American Journal of Obstetrics and Gynecology*, *198*, 590.e1–590.e6. http://dx.doi.org/10.1016/j.ajog.2008.02.022.

Read, C. P., Word, R. A., Ruscheinsky, M. A., Timmons, B. C., & Mahendroo, M. S. (2007). Cervical remodeling during pregnancy and parturition: molecular characterization of the softening phase in mice. *Reproduction*, *134*, 327–340. http://dx.doi.org/10.1530/REP-07-0032.

Robison, K. M., Conway, C. K., Desrosiers, L., Knoepp, L. R., & Miller, K. S. (2017). Biaxial mechanical assessment of the murine vaginal wall using extension–inflation testing. *Journal of Biomechanical Engineering*, *139*, http://dx.doi.org/10.1115/1.4037559.

Robuck, M. F., O'Brien, C. M., Knapp, K. M., Shay, S. D., West, J. D., Newton, J. M., Slaughter, J. C., Paria, B. C., Reese, J., & Herington, J. L. (2018). Monitoring uterine contractility in mice using a transcervical intrauterine pressure catheter. *Reproduction*, *155*, 447–456. http://dx.doi.org/10.1530/REP-17-0647.

Rossi, F., Luppi, S., Fejza, A., Giolo, E., Ricci, G., & Andreuzzi, E. (2025). Extracellular matrix and pregnancy: functions and opportunities caught in the net. *Reproductive Biology and Endocrinology*, *23*, 24. http://dx.doi.org/10.1186/s12958-025-01348-5.

Sanches, J. C. T., Jones, C. J. P., Aplin, J. D., Iozzo, R. V., Zorn, T. M. T., & Oliveira, S. F. (2010). Collagen fibril organization in the pregnant endometrium of decorin-deficient mice. *Journal of Anatomy*, *216*, 144–155. http://dx.doi.org/10.1111/j.1469-7580.2009.01170.x.

Suarez, A. C., Gimenez, C. J., Russell, S. R., Wang, M., Munson, J. M., Myers, K. M., Miller, K. S., Abramowitch, S. D., & De Vita, R. (2024). Pregnancy-induced remodeling of the murine reproductive tract: a longitudinal in vivo magnetic resonance imaging study. *Science Reports*, *14*, 1–19. http://dx.doi.org/10.1038/s41598-023-50437-1.

Teodoro, W. R., Witzel, S. S., Velosa, A. P. P., Shimokomaki, M., Abrahamsohn, P. A., & Zorn, T. M. T. (2003). Increase of interstitial collagen in the mouse endometrium during decidualization. *Connective Tissue Research*, *44*, 96–103. http://dx.doi.org/10.1080/03008200390200238.

Wachsberg, R. H., Kurtz, A. B., Levine, C. D., Solomon, P., & Wapner, R. J. (1994). Real-time ultrasonographic analysis of the normal postpartum uterus: technique, variability, and measurements. *Journal of Ultrasound in Medicine*, *13*, 215–221. http://dx.doi.org/10.7863/jum.1994.13.3.215.

White, S. E., Kiley, J. X., Visniauskas, B., Lindsey, S. H., & Miller, K. S. (2022). Biaxial murine vaginal remodeling with reproductive aging. *Journal of Biomechanical Engineering*, *144*, http://dx.doi.org/10.1115/1.4054362.

Woessner, J., & Brewer, T. (1963). Formation and breakdown of collagen and elastin in the human uterus during pregnancy and post-partum involution. *Biochemical Journal*, *89*, 75–82. http://dx.doi.org/10.1042/bj0890075.

Yoshida, K., Jayyosi, C., Lee, N., Mahendroo, M., & Myers, K. M. (2019). Mechanics of cervical remodelling: insights from rodent models of pregnancy. *Interface Focus*, *9*, Article 20190026. http://dx.doi.org/10.1098/rsfs.2019.0026.

Yoshida, K., Jiang, H., Kim, M., Vink, J., Cremers, S., Paik, D., Wapner, R., Mahendroo, M., & Myers, K. (2014). Quantitative evaluation of collagen crosslinks and corresponding tensile mechanical properties in mouse cervical tissue during normal pregnancy. *PLoS One*, *9*, Article e112391. http://dx.doi.org/10.1371/journal.pone.0112391.

Yoshida, K., Mahendroo, M., Vink, J., Wapner, R., & Myers, K. (2016). Material properties of mouse cervical tissue in normal gestation. *Acta Biomaterials*, *36*, 195–209. http://dx.doi.org/10.1016/j.actbio.2016.03.005.